Heliyon 10 (2024) e30517

Contents lists available at ScienceDirect

Heliyon

journal homepage: www.cell.com/heliyon

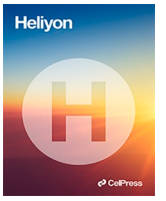

Research article

Identifying the miRNA-gene networks contributes to exploring paravertebral muscle degeneration's underlying pathogenesis and therapy strategy

Yongjin Li [a,b], Wei Wang [a], Chao Kong [a], Xiaolong Chen [a], Chaoyi Li [c,*], Shibao Lu [a,**]

[a] Department of Orthopedics, Xuanwu Hospital, Capital Medical University, No. 45 Changchun Street, Xicheng District, Beijing, China
[b] Spine Center, Department of Orthopaedics, The First Affiliated Hospital of USTC, Division of Life Sciences and Medicine, University of Science and Technology of China, No.17, Lujiang Road, Hefei, Anhui, 230001, China
[c] Department of Joint Surgery, The Second Affiliated Hospital of Hainan Medical University, Haikou, 570311, China

ARTICLE INFO

Keywords:
RNA sequencing
Paravertebral muscle degeneration
Bioinformatics analysis
Differential expression microRNAs
Differential expression genes
Signaling network

ABSTRACT

Low back pain (LBP) is a worldwide problem with public health. Paravertebral muscle degeneration (PMD) is believed to be associated with LBP. Increasing evidence has demonstrated that microRNA (miRNA)-mRNA signaling networks have been implicated in the pathophysiology of diseases. Research suggests that cell death, oxidative stress, inflammatory and immune response, and extracellular matrix (ECM) metabolism are the pathogenesis of PMD; however, the miRNA-mRNA mediated the pathological process of PMD remains elusive. RNA sequencing (RNA-seq) and single cell RNA-seq (scRNA-seq) are invaluable tools for uncovering the functional biology underlying these miRNA and gene expression changes. Using scRNA-seq, we show that multiple immunocytes are presented during PMD, revealing that they may have been implicated with PMD. Additionally, using RNA-seq, we identified 76 differentially expressed genes (DEGs) and 106 differentially expressed miRNAs (DEMs), among which IL-24 and CCDC63 were the top upregulated and downregulated genes in PMD. Comprehensive bioinformatics analyses, including Venn diagrams, differential expression, functional enrichment, and protein-protein interaction analysis, were then conducted to identify six ferroptosis-related DEGs, two oxidative stress-related DEGs, eleven immunity-related DEGs, five ECM-related DEGs, among which AKR1C2/AKR1C3/SIRT1/ALB/IL-24 belong to inflammatory genes. Furthermore, 67 DEMs were predicted to be upstream miRNAs of 25 key DEGs by merging RNA-seq, TargetScan, and mirDIP databases. Finally, a miRNA-gene network was constructed using Cytoscape software and an alluvial plot. ROC curve analysis unveiled multiple key DEGs with the high clinical diagnostic value, providing novel approaches for diagnosing and treating PMD diseases.

1. Introduction

Low back pain (LBP) is a worldwide public health problem that has steadily increased. The socioeconomic burden caused by LBP is huge, accounting for approximately $100 billion in global medical costs per annum [1–3]. The occurrence and progression of LBP are

* Corresponding author.
** Corresponding author.
E-mail addresses: li35499015@126.com (C. Li), shibaolu@xwh.ccmu.edu.cn (S. Lu).

https://doi.org/10.1016/j.heliyon.2024.e30517
Received 1 March 2024; Received in revised form 24 April 2024; Accepted 29 April 2024
Available online 3 May 2024

often the result of spinal structural and functional disorders, such as paravertebral muscle degeneration (PMD) and intervertebral disc degeneration (IVDD) [4–7]. Because of the coordinated movement of the paravertebral muscles (PVM) and the intervertebral discs, the interaction of these elements plays a key role in maintaining the stability of the spinal structure and function [8,9]. Current treatments for LBP include medication and surgery focusing on alleviating pain and its complications. However, these methods rarely focus on solving the root causes of LBP and restoring the normal physiological structure and function of the spine, resulting in unsatisfactory outcomes [1,2,10,11]. Novel therapeutic targets that improve patients' quality of life are urgently needed.

The pathogenesis of IVDD is characterized by distinct inflammatory and immune responses, the increased of cell death, oxidative stress, and extracellular matrix (ECM) degradation, etc [12–16]. Gene therapy, which targets molecules can significantly alleviate IVDD by blocking these pathological processes [12–15]. However, most current investigations only focus on evaluating the morphological parameters of PVM from a clinical point of view [4,5,17–21] and neglect the consideration of the molecular pathological mechanism of PMD. Additionally, studies the on the molecular mechanism of PMD are minimal. Previously, we reported that several genes might regulate PMD in mice via mediating inflammatory response, muscle atrophy, and oxidative stress [22]. Li et al. [23] demonstrated that in patients with idiopathic scoliosis, the PVM undergoes degeneration, leading to increased muscle cell death, loss of muscle function, and spinal instability. Therefore, according to the pathomechanism of IVDD [16] and the research progress of PMD, we speculate that the imbalance of the PVM microenvironment: cell death, oxidative stress, ECM metabolic imbalance, and inflammatory and immune response are key factors contributing to the pathogenesis of PMD (Fig. 1); however, their regulatory mechanisms are still unclear.

Growing evidence has uncovered that the messenger ribonucleic acid (mRNA) and microRNA (miRNA) play a critical role in mediating cell death, ECM metabolism, and immune and inflammatory response [12–16,22]. Disorder of mRNA and miRNA expression is often closely related to the occurrence and development of human diseases, including IVDD and PMD [12–16,22]. Single-cell RNA sequencing (scRNA-seq) has established itself as an invaluable tool for identifying cell types and heterogeneity (such as various immunocytes), as well as differentially expressed genes (DEGs) in isolated single-cells, and elucidating their functions and mechanisms [24–26]. Bulk RNA-seq (bRNA-seq) can also identify differentially expressed miRNAs (DEMs) in tissues, which analyzes the average DEGs or DEMs expression by using tissue as sequencing material; however, the ability to assess the heterogeneity between

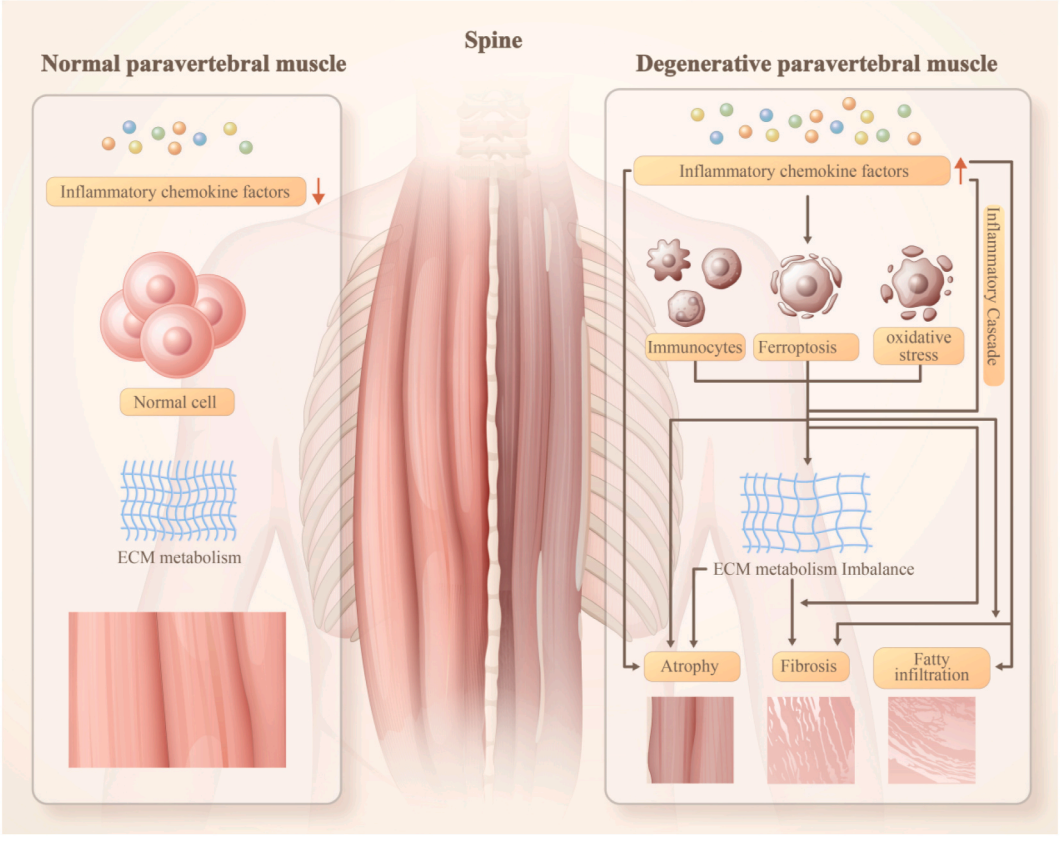

Fig. 1. The pathological mechanism and process of PMD. The left side represents normal paravertebral muscles: reduced expression of inflammatory and chemokine factors, balanced ECM metabolism, normal muscle cell quality, quantity, and muscle structure and function. The right side represents degenerative paravertebral muscles: increased expression of inflammatory and chemokine factors causes ferroptosis, oxidative stress, activation of multiple immunocytes, formation of an inflammatory cascade reaction, promotion of ECM degradation, further leading to muscle atrophy, fibrosis, and fat infiltration, initiating or exacerbating PMD.

cellular cell types is lost [15,16,24]. Few studies have utilized scRNA-seq and bRNA-seq to assess human PVM tissues.

In this study, we conducted scRNA-seq to explore the composition and heterogeneity of immune cells and further identify the key DEGs and DEMs in PMD. First, multiple molecular biology experiments, encompassing Hematoxylin & Eosin (H&E) and Masson's trichrome staining, were carried out to validate whether and to what extent the PVM tissues have degenerated. Second, a series of bioinformatics analyses, such as RNA differential expression analysis, functional enrichment analysis, and protein-protein interaction (PPI) analysis, were performed to predict the key DEGs and DEMs in PMD. Finally, the DEMs-DEGs network was constructed to explore the possible regulatory mechanisms by which muscle degeneration occurs. These data provide novel insights that could develop therapeutic targets for inhibiting PMD and alleviating LBP.

2. Material and methods

2.1. Sample information

The Capital Medical University Xuanwu Hospital Ethics Committee supervised and approved the study protocol (study protocol number: NCT05621494; ethics number: KS2022151-1). Patients who had not received any treatment with LBP for over three months and required surgery were included in the study. In contrast, patients with visceral LBP, acute trauma, infections, tuberculosis, Parkinson's disease, tumors, and a history of lumbar fracture and spinal surgery were excluded from this study. After applying these selection criteria, 10 samples from 10 patients were collected, among which three relatively normal and seven degenerative PVM tissues were used for RNA sequencing, and three relatively normal and one degenerative PVM tissues were used for scRNA-seq. Written informed consent was provided to all patients before they participated. Given that the average muscle cross-sectional area of the L4/5 level is relatively large, muscle samples from this segment were used for further investigation. The Goutellier classification method was applied to evaluate the severity of PMD according to visual semiquantitative of fat infiltration [27–29]. A Goutallier grade 0–1 indicates patients who belong to the normal group, whereas those with grades 2–3 constituted mild PMD (MPMD), and grade 4 constituted the severe PMD (SPMD) group.

2.2. Samples processing and bRNA-seq

The PVM tissues were washed twice using sterile phosphate buffer saline (PBS) and 4 % streptomycin. A sterile surgical knife was then used to remove visible connective tissue, veins, and adipose tissue. Subsequently, the total RNA was extracted using the TRIzol reagent (Life Technologies, USA). NanoPhotometer spectrophotometer and Agilent 2100 bioanalyzer were utilized to evaluate the RNA purity and integrity, respectively. According to the manufacturer's instructions, the NEBNext® UltraTM RNA Library Prep Kit was used to prepare the RNA-seq library. The RNA-seq experiment was performed in the NovelBio Biopharmaceutical Technology Company (Beijing, China).

2.3. Evaluating the rationality of sample selection and grouping

The box and violin plots of mRNA and miRNA unveiled MPMD2 and SPMD1 samples as outliers, indicating that the cells may be dead; while the other eight samples had good consistency, indicating a high similarity in sample composition, which met the standards of subsequent analysis and research (Supplementary Fig. 1a-d). Therefore, we eliminated the two samples and conducted a difference analysis on the remaining three normal PVM samples and five degenerative PVM samples. The density curve plot shows the high expression abundance of mRNAs and miRNAs in different samples (Supplementary Fig. 1e and f), suggesting the differential expression of mRNAs and miRNAs in PMD.

2.4. Analysis of genes and miRNAs expression profile

FastQC software was utilized to assess raw data quality. First, the adapter sequences and low-quality data were removed using Trimmomatic software. BWA software was used to compare clean data to the reference genome sequence from Ensembl database to produce sequence alignment files. Next, the clean miRNA data sequences were compared with annotated known miRNAs in the miRBase database (URL or REF). The relative expression levels of mRNAs were calculated using the Fragments Per Kilobase of exon model per Million mapped fragments (FPKM) formula, and the relative expression levels of miRNAs were calculated by the transcripts per kilobase of exon model per million mapped reads (TKM) formula. Data processing was performed in R version. The false discovery rate (FDR) was used to correct the *P*-values. The differentially expressed genes (DEGs) were analyzed using EBSeq software with the screening threshold set to $|\log2 \text{ fold-change (FC)}| > 0.585$ and the FDR <0.05. Differentially expressed miRNAs (DEMs) were analyzed using EdgeR software with the screening threshold being set to $|\log2 \text{ FC}| > 0.585$ and *P*-value <0.05. Hierarchical Clustering and volcano plots were used to illustrate the distinguishable genes and miRNAs expression patterns among samples.

2.5. Samples processing and scRNA-seq

The processed muscle tissues were digested into a single-cell suspension using a digestive enzyme system [30–32]. The scRNA-seq experiment was performed by the NovelBio Biopharmaceutical Technology Company (Beijing, China). According to the manufacturer's instructions, a 10X Genomics Chromium Controller Instrument and Chromium Single Cell 3′ V3.1 Reagent Kits (10X Genomics,

Pleasanton, CA) were used to construct scRNA-seq libraries. The libraries were then sequenced on an Illumina NovaSeq 6000 platform (Illumina, San Diego, CA). After data quality control, the data was dimensionally reduced through T-distributed Stochastic Neighbor Embedding (t-SNE) processing. Unsupervised cell cluster results were obtained using a graph-based cluster method and K-means algorithm. Clusters representing the various immune cells underwent re-*t*-SNE analysis and graph-based clustering to identify immune cell subtypes further.

2.6. Analysis of the protein-protein interaction (PPI) network

The Search Tool for the Retrieval of Interacting Genes (STRING) online tool (https://string-db.org/) is routinely used by scientists to integrate protein-protein interactions systematically. STRING was used to construct the PPI networks of DEGs [33]. Briefly, the DEGs were inputted into the multiple protein section of the STRING website. The interaction file (string_interactions.tsv) was downloaded and converted to Excel. Next, the file was inputted into Cytoscape (Software details). The maximal clique centrality (MCC) algorithm based on the CytoHubba plugin of Cytoscape software was used to identify essential hub genes.

2.7. Gene ontology (GO) and kyoto encyclopedia of genes and genomes (KEGG) enrichment analysis

GO is an international standardized Gene function classification database that includes Biological Process (BP), Cellular Component (CC), and Molecular Function (MF). Additionally, KEGG pathway analysis uses a gene annotation database to detect signaling pathways with significantly enriched differentially expressed genes. From a biological perspective, BP and KEGG can directly reflect the role of genes in phenotype [15,16,22,34]. CC is often used to describe the localization information of genes on cells. As a description of MF, it is often related to the actual mode of action of the proteins. We carried out GO and KEGG pathway analysis to uncover the underlying functional characteristics of DEGs using Weishengxin, an online platform for data analysis and visualization (http://www.bioinformatics.com.cn/?p=10). The threshold of significance was defined by a *P*-value <0.05.

2.8. Obtaining the ECM-related genes, oxidative stress-related genes, ferroptosis-related genes, and immunity-related genes from databases

ECM-related genes (ERGs) were obtained from the Reactome (Version 79, https://reactome.org/) and the HUGO gene databases [15,16]. Ferroptosis-related genes (FRGs) were obtained from the FerrDb V2 database (http://www.zhounan.org/ferrdb/) [15,16,35]. Oxidative stress-related genes (OSRGs) were obtained from the molecular signatures database (https://www.gsea-msigdb.org/gsea/msigdb/index. jsp) [15,16,36]. Immunity-related genes (IRGs) were obtained from the immunology database and analysis portal (immport, https://www.immport.org/home) (Supplementary Table 1) [15,16,37].

2.9. Identification of the key DEGs

To identify the DEGs related to ferroptosis, oxidative stress, immune response, and ECM metabolism, the FRGs, OSRGs, IRGs, and ERGs were merged with DEGs using a Venn diagram, screening for overlapping genes. PPI network analysis was also performed to explore the key hub genes.

2.10. Predicting the upstream DEMs for the key DEGs

For the key DEGs identified above, upstream miRNAs of the key DEGs were predicted using TargetScan version 8.0 (https://www.targetscan.org/) [38] and mirDIP version 5.2 databases [39], respectively. Then, PMD-related DEMs were further selected by merging RNA sequencing-identified DEMs and TargetScan and mirDIP databases.

2.11. Construction of miRNA-gene regulatory network

Next, the miRNA-gene regulatory network was constructed. The process involved analyzing the expression profiles of genes and miRNAs to identify DEMs and DEGs. Special attention was given to pinpointing pivotal DEGs associated with PMD and their connections to ferroptosis, oxidative stress, immune response, and ECM metabolism. The next step involved predicting upstream PMD-related DEMs corresponding to the identified key DEGs using TargetScan, mirDIP databases, and RNA sequencing data. Finally, a comprehensive miRNA-gene regulatory network was formulated utilizing Cytoscape software, integrating the insights from the above analyses.

2.12. Analysis of receiver operating characteristic (ROC) curve

The pROC package deployed in R was applied to carry out ROC curve analysis [40]. Through the analysis, the specificity and sensitivity of key genes could be predicted. The area under the ROC curve (AUC) was used to assess the diagnostic values of the genes.

2.13. H&E and Masson's trichrome staining

Human PVM tissues were fixed and collected at L4/5 level in 4 % paraformaldehyde, followed by dehydrating them with different

concentrations of ethanol. The tissues were then embedded in paraffin and cut into 5 μm thick slices using sterile scissors. Next, xylene was used for dewaxing, followed by hydration of the tissues with different ethanol concentrations. Subsequently, the tissue slices were stained using H&E and Masson's trichrome staining reagent kits, respectively. Cell nuclei were labeled blue using 4′,6-diamidino-2-phenylindole (DAPI). The stained samples were imaged using a fluorescence microscope (Instrument details).

3. Results

3.1. Verifying the normal and degenerative PVM tissues

To study the miRNA-mRNA pathway-mediated the occurrence and development of PMD, we collected normal and degenerative PVM tissues for bRNA-seq and scRNA-seq. Using these tissues and sequencing modalities, we aimed to uncover the expression pattern of genes and miRNAs during PMD (Fig. 2). Through H&E staining, we noted muscle fiber atrophy, local infiltration of adipocytes, and inflammatory cells in degenerative PVM tissues compared with normal PVM tissues (Fig. 3). Masson's trichrome staining further demonstrated many blue-stained collagen fibers crisscrossing the muscles in the degenerative PVM tissues (Fig. 3). Together, these data indicate that the normal and degenerative PVM tissues we collected are suitable for sequencing.

3.2. Single-cell analysis of PVM identifies the types and subtypes of immunocytes

Increasingly, studies have demonstrated that skeletal muscles host multiple immune cells, including monocytes, macrophages, NK cells, neutrophils, B cells, and T cells, using scRNA-seq technology [31,32,41–44]. The same cell clusters have similar gene expression characteristics, but these clusters need to be annotated by cells to determine which cell type they belong to. To identify the immunocytes types in the PVM tissues, we used the tSNE dimensionality reduction strategy to cluster and visualize all cell clusters (Fig. 4a). According to the characteristic marker genes of each cell, we observed a total of 22 clusters representing 10 cell types containing 6 clusters representing four immune cell types, namely monocytic&Neutrophils (clusters 13, 16, 21; 6.82 %; marker genes: C1QA, LYVE1, S100A9); B cells (clusters 20; 0.05 %; marker genes: CD79A, CD79B, IGHM); Mast cells (clusters 17; 1.77 %; marker genes: KIT, CPA3, MS4A2); and T cells (clusters 7; 5.94 %; marker genes: PTPRC, CD3D, CD3E) (Fig. 4, Supplementary Fig. 2, and Supplementary Fig. 3). To further clarify the subtypes of these immune cells, we conducted t-SNE dimensionality reduction analysis again. Similar to previous studies, we found monocytic were divided into 9 clusters containing four cell types: monocytes (marker genes: FCN1, VCAN, G0S2, S100A8); macrophages (C1QA, C1QB, C1QC, TNF, HMOX1, MAF, OLR1, HSPA6); cCD1 and cCD2 (CLEC9A, WDFY4, IDO1, CCL22, CD1C, FCER1A). Neutrophils (FCGR3B, CSF3R, G0S2, CAMP, LTF, MPO). CD4 T cells: Navie (SELL, CCR7, TCF7); Effector

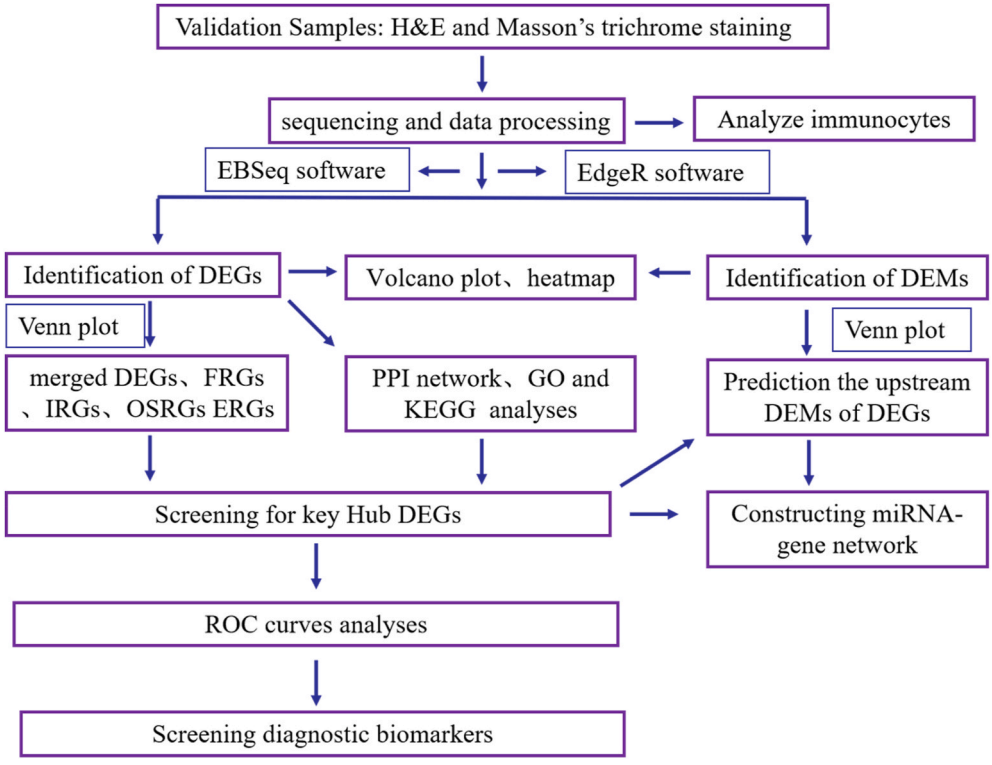

Fig. 2. The workflow diagram of sequencing, data processing, analysis, and validation in this study.

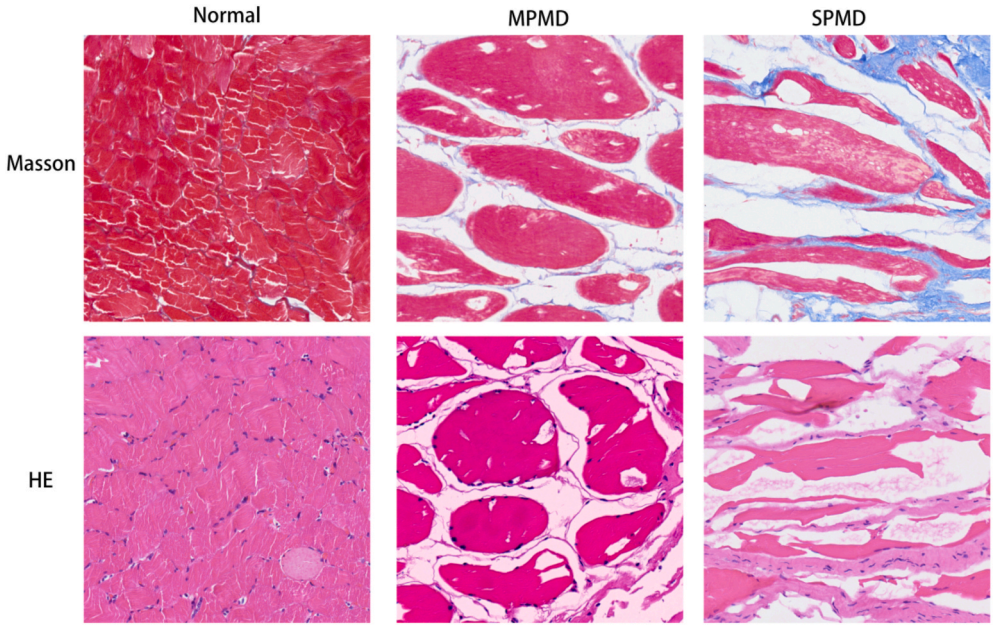

Fig. 3. Histological staining of the normal and degenerative paravertebral muscle tissues. HE and Masson's trichrome staining was conducted to select and confirm the normal, mild, degenerative, and severe degenerative paravertebral muscle tissues.

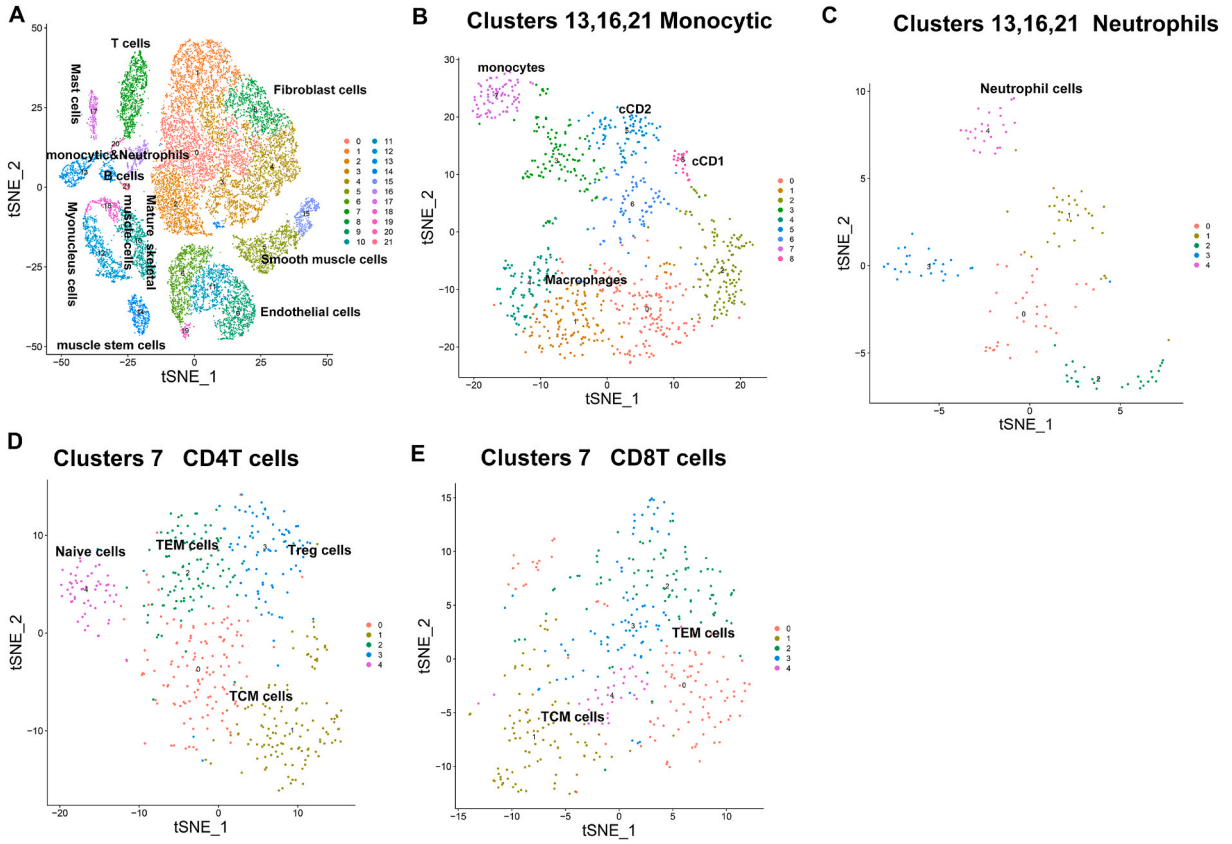

Fig. 4. Identifying the cell types and subtypes of immunocytes in PVM using scRNA-seq. (A) Graph-based clustering of single-cells identifies 22 clusters and 10 cell types using the t-SNE dimensionality reduction method. (B–E) After t-SNE localization, Graph-based unsupervised clustering of immunocytes identified multiple subtypes, including monocytes, macrophages, cCD1, cCD2, Neutrophils, Navie TEM, Treg, TCM.

memory T cells (TEM) (GZMK, GZMA, CCL5); Regulatory T cells (Treg) (FOXP3, IKZF2, CTLA4, BATF); Central memory T cells (TCM) (CD69, RGS1, ANXA1). and CD8T cells: TEM (GZMK, CXCR4, CD44); TCM (IL7R, GPR183, CCL5) (Fig. 4) based on their marker genes [45]. Thus, these results suggested that there are multiple immune cells present during PMD, revealing that they may play an important role in regulating PMD. However, the mechanism remains unclear.

3.3. Identification of the key DEGs in PMD

A total of 15 458 genes were found to be expressed to varying degrees in PMD. Subsequently, we performed gene differential expression analysis to compare gene expression differences between the normal and PMD groups. The screening threshold was set as $|\log2(FC)| > 0.585$ and FDR <0.05. From this analysis, we identified 76 DEGs, among which 43 DEGs were significantly downregulated and 33 were significantly upregulated in human PMD patients, as shown through hierarchical clustering and volcano plotting (Fig. 5a and b). To analyze whether the DEGs are related to ferroptosis, oxidative stress, immune response, and ECM metabolism, we obtained the FRGs, OSRGs, IRGs, and ERGs from the different databases and merged them with DEGs using a Venn diagram (Fig. 5c). The results showed that six were DEGs linked to ferroptosis (leucine-rich adaptor protein 1-like (LURAP1L), aldo-keto reductases family 1 member C2 (AKR1C2), AKR1C3, sirtuin 1 (SIRT1), bromodomain-containing protein 2 (BRD2), albumin (ALB)); two were associated with oxidative stress (peroxidasins (PXN), haptoglobin (HP)); 11 were related to immune response (solute carrier family 45 member 3 (SLC45A3), angiotensin-converting enzyme (ACE), quinolinic acid phosphoribosyltransferase (QPRT), rho guanine nucleotide exchange factor 37 (ARHGEF37), amphiphysin (AMPH), protein phosphatase 1 regulatory inhibitor subunit 16 B (PPP1R16 B), FMS-like tyrosine kinase 4 (FLT4), ras-like protein family member 12 (RASL12), FK506-binding protein 11 (FKBP11), CD7, interleukin-24 (IL-24)); and five belonged to ECM-related genes (secreted phosphoprotein 1 (SPP1), fibrinogen A alpha-chain gene (FGA), fibrinogen gamma-chain gene (FGG), intercellular adhesion molecule 4 (ICAM4), matrix metalloproteinase-15 (MMP15)) (Fig. 5c and

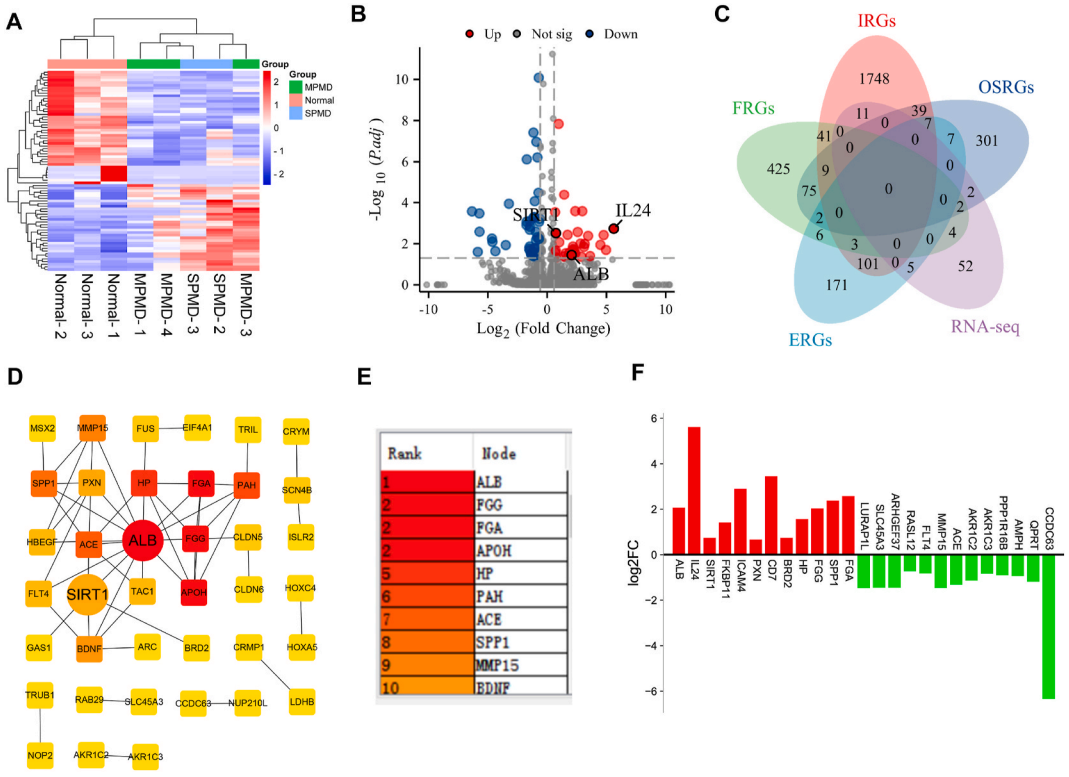

Fig. 5. Analyzing differential gene expression profiles in human PMD patients. (A) Hierarchical clustering plot. Rows represent DEGs, and columns represent different samples. (B) Volcano plot. Blue points represent downregulation (left side), grey points represent insignificant differentially expressed genes (middle), and red points represent upregulation (right side). SIRT1, ALB, and IL-24 were indicated. (C) Screening for DEGs related to ferroptosis, oxidative stress, immune response, and ECM metabolism by Venn plot. (D) The protein–protein interaction network composed of DEGs is visualized by Cytoscape software. The line connecting two nodes represents the interaction between the two genes. The key nodes in the PPI network can be analyzed as key genes. The depth of the nodes color is related to the association of other genes in the PPI network; the color from light to dark represents that the gene is increasingly associated with other genes. Red represents the most key hub genes. (E) The top ten hub genes were screened by the CytoHubba plugin, and were ranked by the maximal clique centrality method and the depth of the nodes color. (F) Bar plot. The X-axis shows the 12 upregulated DEGs and 13 downregulated DEGs, and the Y-axis represents log2 fold change. Red means up-regulation above the X-axis; green means down-regulation below the X-axis. (For interpretation of the references to color in this figure legend, the reader is referred to the Web version of this article.)

Supplementary Table 1).

Many complexities within cells stem from functional and regulatory interactions among proteins, which PPI can reflect. We explored the interactions among the 76 DEGs using the STRING tool and obtained a PPI network. PPI analysis revealed that ALB, FGA, FGG, HP, ACE, SPP1, and MMP15 belonged to the ranking's top 10 key hub genes (Fig. 5d and e). Moreover, the specific expression of

Fig. 6. GO functional annotation of DEGs. (A) Sankey and bubble plots unveil the results of biological processes terms enriched by GO analysis. (B) Sankey and bubble plots unveil the results of cellular components terms enriched by GO analysis. The left is a Sankey plot, representing the DEGs enriched in each pathway; the right is a bubble plot, while the bubble size represents the number of involved DEGs that the pathway belongs to, and the bubble color represents the *P*-value, with red representing greater significance. (For interpretation of the references to color in this figure legend, the reader is referred to the Web version of this article.)

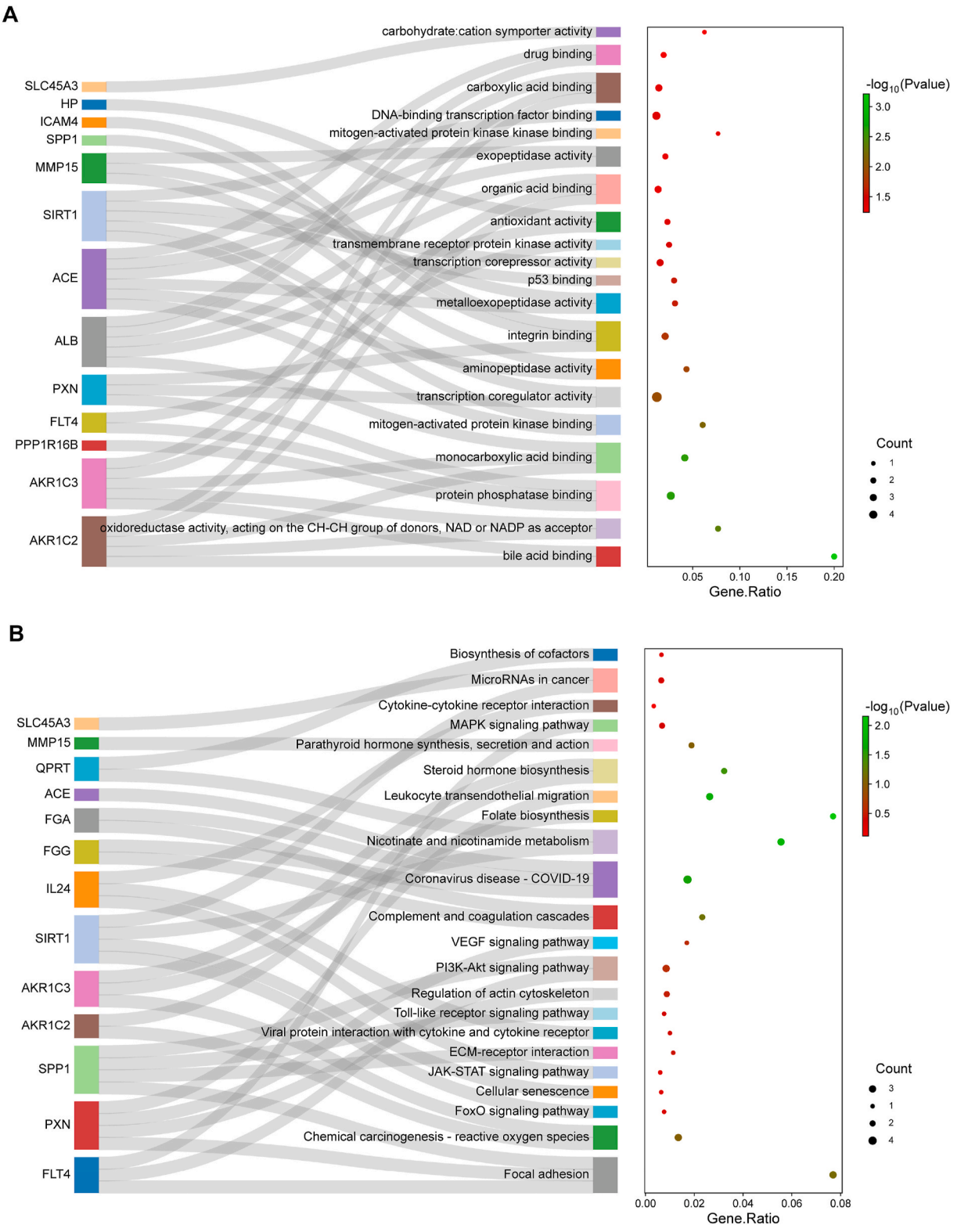

(caption on next page)

Fig. 7. GO and KEGG functional annotation of DEGs. (A) Sankey and bubble plots unveil the results of molecular function terms enriched by GO analysis. (B) Sankey and bubble plots unveil the enriched signaling pathway by KEGG analysis. The left is a Sankey plot, representing the DEGs enriched in each pathway; the right is a bubble plot, while the bubble size represents the number of involved DEGs that the pathway belongs to, and the bubble color represents the *P*-value, with red representing greater significance. (For interpretation of the references to color in this figure legend, the reader is referred to the Web version of this article.)

these DEGs in PMD was further visualized using a bar plot (Fig. 5f). These data indicated that IL-24 and coiled-coil domain-containing protein 63 (CCDC63) were the top upregulated and downregulated genes in PMD, respectively. Additionally, ALB, SIRT1, FKBP11, ICAM4, PXN, CD7, BRD2, HP, SPP1, FGA, FGG were significantly upregulated, and LURAP1L, AKR1C2, AKR1C3, SLC45A3, ACE, QPRT, ARHGEF37, AMPH, PPP1R16 B, FLT4, RASL12, MMP15 were significantly downregulated in PMD.

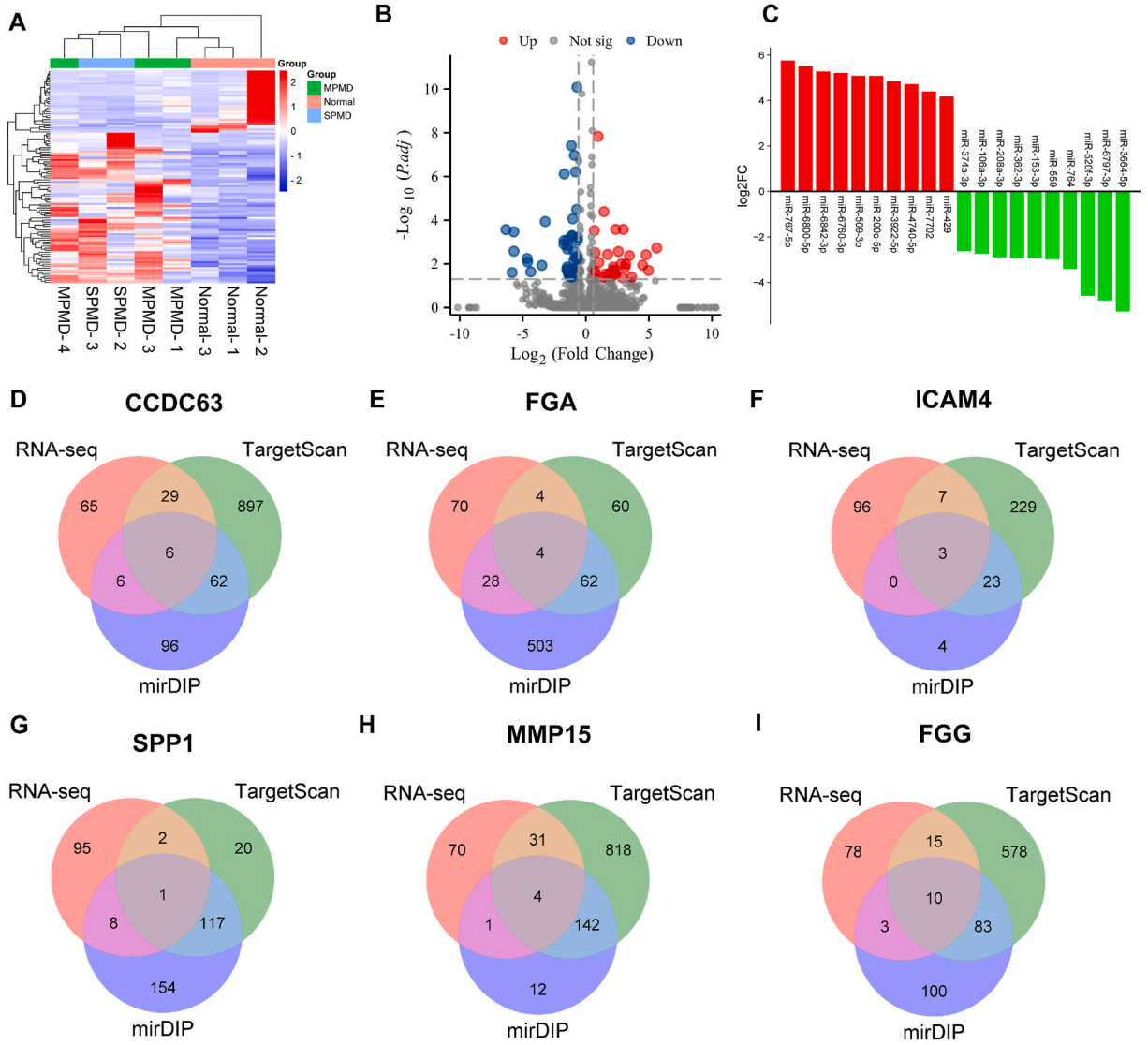

Fig. 8. Analysis of the expression profiles of miRNAs in PMD by RNA-sequencing. (A) Cluster heatmap of DEMs in RNA-seq. With rows indicating DEMs and columns indicating groups. The color scale varies from blue to red; blue points indicate downregulation, and red points indicate upregulation. (B) Volcano plot of DEMs in RNA-seq. Red points indicate significantly upregulation; blue points indicate significantly down-regulation, grey points indicate insignificant differential expression. (c) bar plot of DEMs in RNA-seq. The X-axis represents miRNA, and the Y-axis represents log2 fold change. Green means down-regulation below the X-axis; red means up-regulation above the X-axis. (D–I) Venn diagram analysis of overlapping ECM-related DEMs by the intersection of ERGs, TargetScan, and mirDIP databases. (For interpretation of the references to color in this figure legend, the reader is referred to the Web version of this article.)

3.4. GO and KEGG functional annotation of DEGs

To further explore the underlying functional characteristics of the 76 DEGs, GO and KEGG enrichment analyses were carried out using Weishengxin, an online data analysis and visualization platform. The GO and KEGG results revealed that FGG/FGA/ALB are linked to "regulation of vasoconstriction, protein activation cascade, regulation of endothelial cell apoptotic process, post-translational protein modification, negative regulation of apoptotic signaling pathway, substrate adhesion-dependent cell spreading, extracellular matrix organization, protein processing, regulation of cell morphogenesis involved in differentiation, positive regulation of heterotypic cell-cell adhesion, complement and coagulation cascades, coronavirus disease-COVID-19, collagen-containing extracellular matrix, blood microparticle, and cytoplasmic vesicle lumen". AKR1C2/AKR1C3/SIRT1/ALB are related to "regulation of protein kinase B signaling, cellular response to ketone, regulation of endothelial cell apoptotic process, cellular response to external stimulus, cellular response to starvation, response to reactive oxygen species, chemical carcinogenesis-reactive oxygen species, steroid hormone biosynthesis, oxidoreductase activity, acting on the CH–CH group of donors, NAD or NADP as acceptor, bile acid, monocarboxylic acid, organic acid, and carboxylic acid binding". SIRT1 is correlated to "epithelial cell migration, regulation of cell growth, endothelial cell proliferation, cellular response to transforming growth factor beta stimulus, negative regulation of apoptotic signaling pathway, FoxO signaling pathway, Cellular senescence, ESC/E(Z) complex, nuclear euchromatin, mitogen-activated protein kinase binding, transcription coregulator activity, p53 binding, transcription corepressor activity, DNA-binding transcription factor binding, etc". IL-24 is associated with "peptidyl tyrosine phosphorylation, JAK-STAT signaling pathway, viral protein interaction with cytokine and cytokine receptor, cytokine-cytokine receptor interaction". FLT4/PXN/SPP1 participate in "epithelial cell migration, regulation of cell growth, Focal adhesion, PI3K-Akt signaling pathway, Toll-like receptor signaling pathway, VEGF signaling pathway, ECM-receptor interaction, Regulation of actin cytoskeleton, cell-cell junction, and integrin binding". MMP15/FGG/SPP1/FGA/ICAM4 regulates extracellular matrix organization (Figs. 6 and 7). These results indicate that AKR1C2/AKR1C3/SIRT1/ALB/IL-24 belong to inflammatory genes and that the above 25 key genes might play a significant role in the occurrence and progression of PMD.

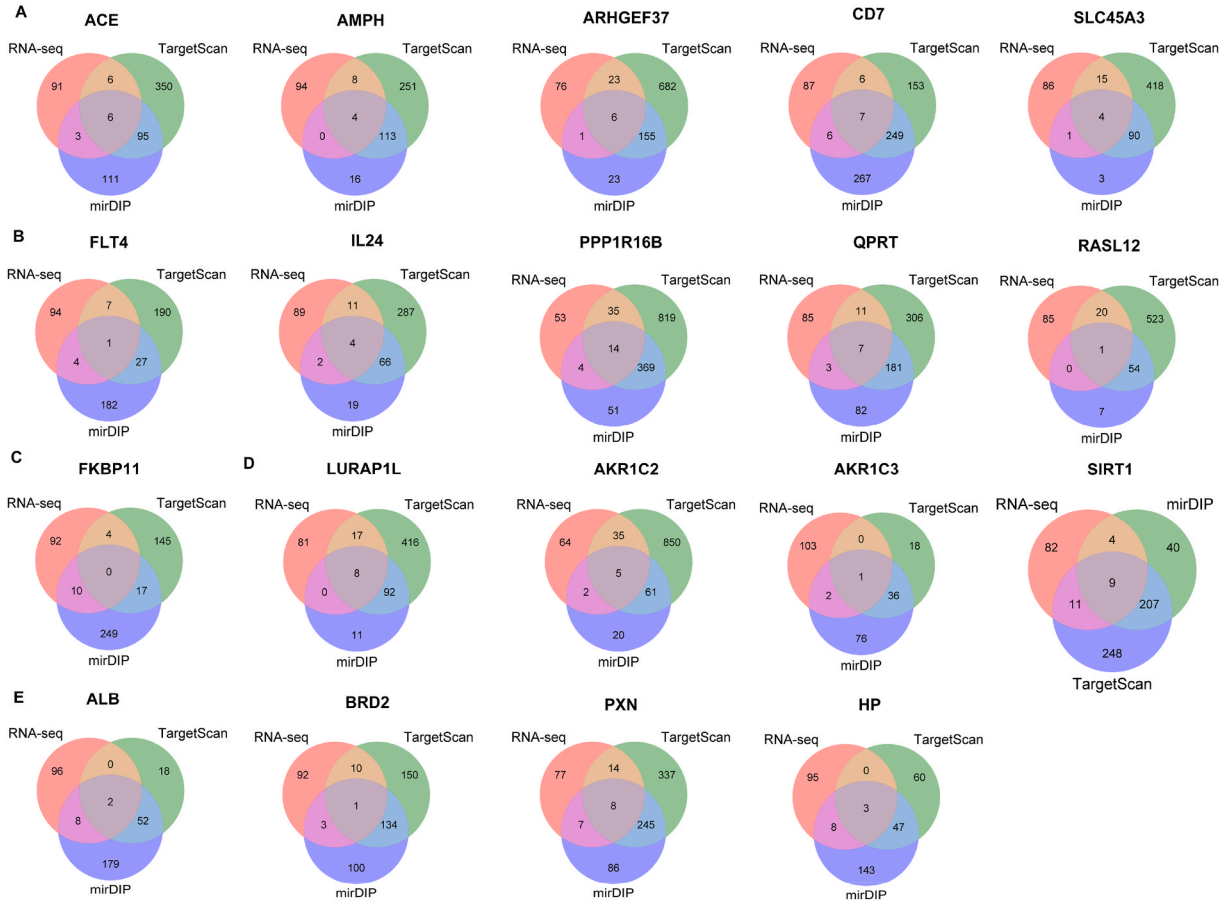

Fig. 9. Predicting the upstream DEMs for the key IRGs, FRGs, and OSRGs. (A–C) Venn diagram analysis of overlapping immunity-related DEMs by the intersection of IRGs, TargetScan, and mirDIP databases. (D) Venn diagram analysis of overlapping ferroptosis-related DEMs by the intersection of FRGs, TargetScan, and mirDIP databases. (E) Venn diagram analysis of overlapping oxidative stress-related DEMs by the intersection of OSRGs, TargetScan, and mirDIP databases.

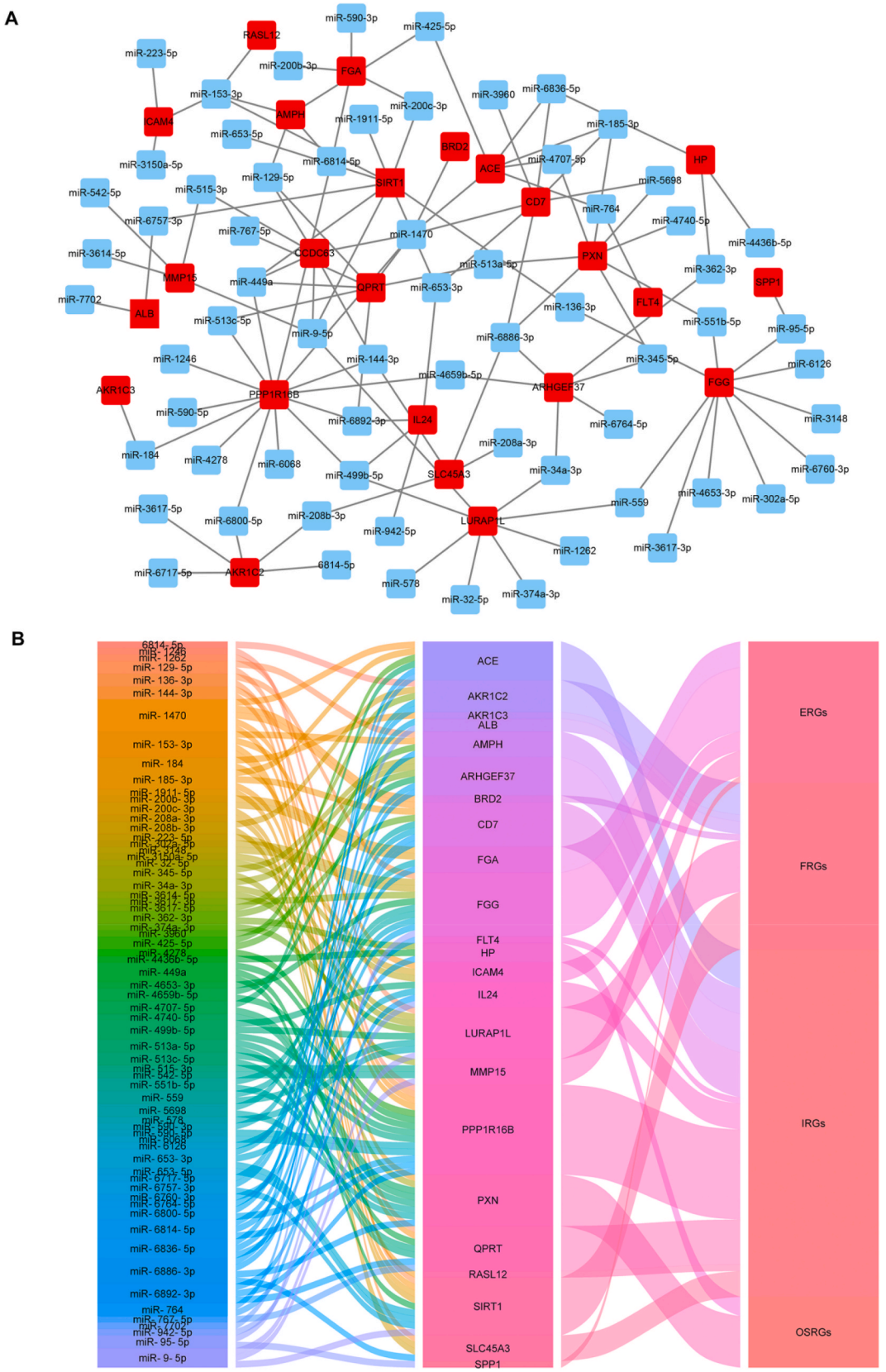

(caption on next page)

Fig. 10. Construction of miRNA-genes regulatory network in PMD. (A) Cytoscape software was used to construct and visualize the miRNA-genes regulatory network. Of these, 25 DEGs are marked in red, and 67 DEMs are marked in blue. (B) Alluvial plot. The left column indicates DEMs, the middle column indicates key DEGs, and the right column indicates the functions of key DEGs. (For interpretation of the references to color in this figure legend, the reader is referred to the Web version of this article.)

3.5. Identification of DEMs in PMD

As the gene expression regulator, miRNAs play a significant role in modulating the occurrence and development of diseases via targeting and binding genes [46,47]. RNA sequencing identified a total of 1610 miRNAs. As shown in the volcano plot (Fig. 8a) and cluster heatmap (Fig. 8b), we found 106 miRNAs with | log2 FC | > 0.585 and P value < 0.05, of which 75 were significantly upregulated and 31 were significantly downregulated in PMD. The differential expression of the top 10 upregulated and top 10 downregulated DEMs was shown using a bar plot (Fig. 8c), of which miR-767-5p was the top upregulated, and miR-3664-5p was the top downregulated DEMs in PMD, respectively. These data revealed that these DEMs might be implicated in PMD.

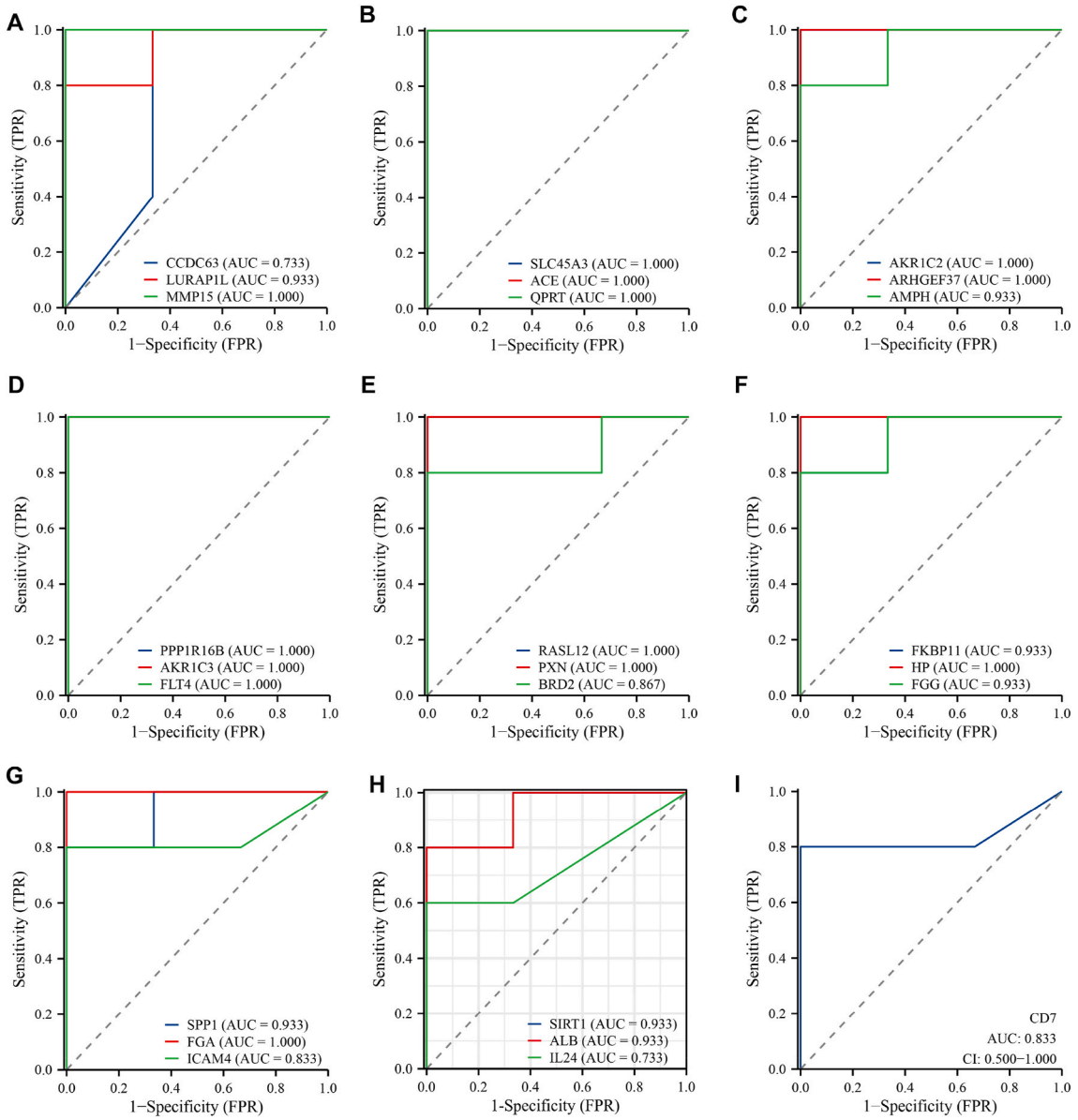

Fig. 11. Evaluation of the diagnostic effectiveness of the key DEGs in PMD. (A–I) Analyzing the ROC curve and AUC value of 25 key DEGs based on the sequencing data. The abscissa represents 1-specificity, and the closer the value is to zero, the higher the accuracy. The vertical axis represents sensitivity; the larger the value, the better the accuracy.

3.6. Predicting the upstream DEMs for the key DEGs

TargetScan version 8.0 (https://www.targetscan.org/) [38] predicts the target genes that match the seed region of each miRNA. These predictions can then be ranked using a miRNA-mediated inhibition biochemical model. MirDIP version 5.2 (https://ophid.utoronto.ca/mirDIP) [39] is a comprehensive and updated database that includes 46 364 047 predictions for 2734 miRNAs and 27 936 genes, which collects human miRNA-gene interactions from multiple known databases, such as miRDB, miRanda, miRbase, miRcode, RNA22, miRTar2GO, and PITA. Concerning the 25 key DEGs and 106 DEMs acquired through RNA sequencing, we conducted predictions to identify the upstream DEMs associated with PMD among the key DEGs. This prediction process involved integrating RNA-seq data with TargetScan and mirDIP database information. The upstream DEMs of the key DEGs were listed in Supplementary Table 2. The most significantly downregulated CCDC63 was predicted to have 6 DEMs (Fig. 8d). As for ECM-related DEGs, we predicted that FGA, ICAM4, SPP1, MMP15, and FGG have 4 + 3+1 + 4+10 (22) overlapping DEMs, respectively (Fig. 8e–i). A total of 6 + 4+6 + 7+1 + 4+14 + 7+0 + 1+4 (54) overlapping DEMs were predicted as upstream miRNAs of 11 immune-related DEGs (Fig. 9a–c). Additionally, six ferroptosis-related DEGs had 8 + 1+5 + 9+1 + 2 (26) upstream DEMs through Venn analysis, respectively; two oxidative stress-related DEGs, PXN and HP were believed to have eight and three upstream overlapping DEMs, respectively (Fig. 9d and e).

3.7. Construction of miRNA-gene regulatory network

Based on the above prediction analysis, 67 DEMs were predicted to be upstream miRNAs of 25 key DEGs, excluding the same 52 DEMs. Then, we constructed and visualized a miRNA-gene regulatory network containing 67 DEMs and 25 DEGs using Cytoscape and further illustrated these data using an alluvial plot (Fig. 10a and b). From the interlocking miRNA-gene signaling regulatory networks, we can observe that multiple miRNAs can regulate the same gene, and the same miRNA can also mediate multiple genes (Fig. 10a and b). The alluvial plot also reflected the potential biological role of miRNA-gene networks in PMD (Fig. 10b). These results unveiled that miRNA-gene signaling networks might be involved in the occurrence and progression of PMD by regulating ferroptosis, immune response, ECM metabolism, and oxidative stress.

3.8. Evaluation of the diagnostic values of key DEGs

The ROC curve reflects the relationship between sensitivity and specificity [40,43]. The ROC AUC curve is commonly used to evaluate the diagnostic value of different genes. The AUC value range is generally between 0.5 and 1, and the closer the AUC is to 1, the better the prediction effect of this variable [40,43]. An AUC of more than 0.9 was considered capable of diagnosing PMD with excellent specificity and sensitivity. According to the key DEGs identified in this study, we conducted a ROC curve analysis using R to evaluate the clinical diagnostic value of these genes. As shown in Fig. 11, the AUC values of MMP15, SLC45A3, ACE, QPRT, AKR1C2, ARHGEF37, PPP1R16 B, FLT4, AKR1C3, RASL12, PXN, HP, FGA were 1. The AUC values of LURAP1L, AMPH, FKBP11, FGG, SPP1, SIRT1, and ALB were greater than 0.9. However, the AUC values of CCDC63, IL-24, CD7, ICAM4, and BRD2 were less than 0.9 (Fig. 11a–e, g, h, i). These data revealed that MMP15, SLC45A3, ACE, QPRT, AKR1C2, ARHGEF37, PPP1R16 B, FLT4, AKR1C3, RASL12, PXN, HP, FGA, LURAP1L, AMPH, FKBP11, FGG, SPP1, SIRT1, and ALB have excellent specificity and sensitivity, and have high diagnostic value for PMD and could be used as diagnostic biomarkers for further analysis and validation.

4. Discussion

Current studies on PMD predominantly focus on measuring PVM morphological parameters, such as cross-sectional area size and fat infiltration degree [4,5,17–21]. However, the pathomechanism of PMD is poorly understood, limiting clinical application and translation. bRNA-seq and scRNA-seq are robust tools and common methods to identify key molecular pathological mechanisms underlying disease conditions [24–26]. Gene therapy targeting miRNA or mRNA has high efficiency and specificity, which can achieve precise treatment, improve microenvironment homeostasis, and treat muscle degenerative diseases from the root cause [48]. However, few studies have investigated human PVM tissues using bRNA-seq and scRNA-seq, which both have the potential to illuminate critical biological and pathological insights. Therefore, it is necessary to use sequencing technology to understand and elucidate the pathogenesis of PMD from a genetic perspective.

In this study, we identified 76 DEGs (43 downregulated and 33 upregulated), of which IL-24 and CCDC63 were the most significantly upregulated and downregulated in PMD. Among them, we identified six FRGs: LURAP1L, AKR1C2, AKR1C3, SIRT1, BRD2, and ALB; two OSRGs: PXN, HP; 11 IRGs: SLC45A3, ACE, QPRT, ARHGEF37, AMPH, PPP1R16 B, FLT4, RASL12, FKBP11, CD7, and IL-24; 5 ERGs: SPP1, FGA, FGG, ICAM4, and MMP15; and five inflammatory genes: AKR1C2, AKR1C3, SIRT1, ALB, and IL-24. Together, these results revealed that DEGs-mediated ferroptosis, oxidative stress, ECM metabolism, and inflammatory and immune response might be the key pathological processes of PMD.

ECM not only protects muscle cells and blood vessels but also exerts a crucial role in the growth, development, and repair of skeletal muscles, as well as in transmitting muscle contractile force [49,50]. Thus, ERGs may play an extremely important role in maintaining muscle homeostasis and function by regulating the content of ECM components. Nevertheless, how do ERGs mediate ECM metabolism? To clarify this issue, we have consulted relevant literature. We observed MMP15, an ECM degradation metallopeptidase, is differentially expressed in skeletal muscles during exercise, which is associated with ECM remodeling [51]. Kramerova et al. discovered that SPP1 could promote muscle fibrosis and macrophage polarization by inducing MMP9-mediated ECM degradation [52]. Inflammatory

response and oxidative stress were also reported to enhance ECM degradation [12,16]. We found that AKR1C2/AKR1C3/SIRT1/ALB/IL-24 are associated with inflammatory responses, and PXN/HP are linked to oxidative stress through genes function enrichment analysis, suggesting that they may affect the expression of ECM components in PMD. Accumulating evidence has revealed that SIRT1 is essential in inhibiting inflammation and oxidative stress, thereby repressing ECM degradation [53]. IL-24 belongs to the IL-10 cytokine family, which can be promoted by fibrosis interfering with ECM metabolism [54]. Our study also found that FGG/FGA/ICAM4 were linked to ECM deposition and remodeling. Taken together, we speculated that many DEGs can regulate the occurrence and development of PMD via controling ECM metabolism.

Immune system disorders such as immunocyte activation and immune-related gene dysregulation are important features of skeletal muscle diseases. Researchers observed that there are five immunocytes: macrophages, monocytes, neutrophils, and B/T cells in adult mouse hindlimb muscles by scRNA-seq [32,44]. In another scRNA-seq study, De Micheli et al. [31,42] found myeloid immunocytes, tissue-resident and anti-inflammatory macrophages, pro-inflammatory macrophages and monocytes, B/T cells and NK cells in human and mouse skeletal muscles. Similar to human and animal skeletal muscle scRNA-seq results, we identified mast cells, monocytic cells, B/T cells in human PVM. Among them, the proportion of monocytes is the highest, accounting for 6.82 %; Mast cells account for 1.77 %; T cells account for 5.94 %; and B cells have the lowest proportion at approximately 0.05 %. Furthermore, Xu et al. [41] detected that T cells account for 4.08 %, neutrophils account for 3.34 %, and B cells account for 0.71 % in glycerol-treated skeletal muscle. However, the study on the analysis of immunocytes subtypes in skeletal muscle is still very limited. In this study, we identified nine immunocytes subtypes: monocytes, macrophages, cCD1, cCD2, neutrophils, Navie, TEM, Treg, and TCM.

As a group of non-coding RNAs, miRNAs cannot encode proteins but are potent genetic regulatory factors because a single miRNA can regulate multiple signaling pathways by targeting a series of target genes [12–16,55]. More importantly, a large body of clinical and animal trials indicated that miRNAs not only act as potential biomarkers for diagnosis and prognosis but also have been shown to have therapeutic value for diseases [45,46,56,57]. Few studies have reported miRNAs which mediate the pathological process of PMD. In this present study, we discovered 106 DEMs during PMD. Among these, miR-767-5p was the top-upregulated DEM, and miR-3664-5p was the top-downregulated DEM in PMD. Notably, the most significantly downregulated differentially expressed gene, CCDC63, was predicted to be a target gene of miR-767-5p. Furthermore, we assembled a regulatory network comprising 67 DEMs and 25 DEGs, suggesting their potential involvement in PMD. Nevertheless, the functions and biological significance of these key DEMs in PMD remains unknown and needs further verification.

This study has several noteworthy limitations. First, the clinical sample size collected for sequencing was relatively small, which might affect the conclusions. More samples need to be collected to validate the generalizability and reproducibility of our findings. Second, a flow cytometry experiment and fluorescence-activated cell sorting strategy should be used to identify and isolate key immunocytes, such as macrophages, from PVM tissues to further validate the conclusions made here. Third, functional verification experiments of key genes and miRNAs in immunocytes need to be performed in the future, as most of the results presented here are based on predictive models. Finally, we only studied PVM at the L4-5 segment, and the PVM at other segments should be included in future studies to better identify the pathological mechanism of PMD.

5. Conclusion

In summary, this study assessed the pathomechanism of PMD using scRNA-seq and bRNA-seq. We found four immunocytes, including mast cells, monocytes, and B/T cells, as well as nine immunocyte subpopulations such as monocytes, macrophages, cCD1, cCD2, neutrophils, Navie, TEM, Treg, TCM in human PVM. Additionally, we identified 76 DEGs and 106 DEMs using RNA-seq, among which IL-24/miR-767-5p and CCDC63/miR-3664-5p were the most significantly upregulated and downregulated DEGs/DEMs in PMD. Based on these data, a DEMs-DEGs network was constructed, comprising 67 DEMs and 25 DEGs associated with ferroptosis, oxidative stress, ECM metabolism, and inflammatory and immune response. ROC curve analysis revelaed that MMP15, SLC45A3, ACE, QPRT, AKR1C2, ARHGEF37, PPP1R16 B, FLT4, AKR1C3, RASL12, PXN, HP, FGA, LURAP1L, AMPH, FKBP11, FGG, SPP1, SIRT1, and ALB have high diagnostic value for PMD. These results provide new insights into PMD pathomechanism, diagnosis, and treatment opinions.

Ethics statement

We abide to the Cell Press Editorial Ethics policies as well as Elsevier's Publishing Ethics policies. This study involving human samples were performed in compliance with relevant laws and institutional guidelines such as The Code of Ethics of the World Medical Association (Declaration of Helsinki) and that the Capital Medical University Xuanwu Hospital Ethics Committee have approved them (ethics number: KS2022151-1). The informed consent was obtained for RNA sequencing with human subjects. The privacy rights of human subjects must always be observed.

Funding

This study including sample processing, data collection and analysis was funded by National Natural Youth Cultivation Project of Xuanwu Hospital of Capital Medical University (QNPY2022022), Beijing Postdoctoral Research Foundation (2023-ZZ-024), and the key Science and Technology Project of Beijing Municipal Education Commission (KZ20231002537).

Data availability statement

The data associated with our study has not been deposited into a publicly available repository, and the data will be made available on request.

CRediT authorship contribution statement

Yongjin Li: Writing – original draft. **Wei Wang:** Investigation. **Chao Kong:** Validation. **Xiaolong Chen:** Writing – review & editing. **Chaoyi Li:** Writing – review & editing. **Shibao Lu:** Writing – review & editing.

Declaration of AI and AI-assisted technologies in the writing process

Not Applicable.

Declaration of competing interest

The authors declare no competing interests.

Acknowledgements

The authors would like to thank all the reviewers who participated in the review, as well as MJEditor (www.mjeditor.com) for providing English editing services during the preparation of this manuscript.

Appendix A. Supplementary data

Supplementary data to this article can be found online at https://doi.org/10.1016/j.heliyon.2024.e30517.

References

[1] A. Chiarotto, B.W. Koes, Nonspecific low back pain, N. Engl. J. Med. 386 (2022) 1732–1740, https://doi.org/10.1056/NEJMcp2032396.
[2] N.N. Knezevic, K.D. Candido, J.W.S. Vlaeyen, J. Van Zundert, S.P. Cohen, Low back pain, Lancet 398 (2021) 78–92, https://doi.org/10.1016/S0140-6736(21)00733-9.
[3] J.L. Dieleman, J. Cao, A. Chapin, C. Chen, Z. Li, A. Liu, C. Horst, A. Kaldjian, T. Matyasz, K.W. Scott, A.L. Bui, M. Campbell, H.C. Duber, A.C. Dunn, A. D. Flaxman, C. Fitzmaurice, M. Naghavi, N. Sadat, P. Shieh, E. Squires, K. Yeung, C.J.L. Murray, US health care spending by payer and health condition, 1996-2016, JAMA 323 (2020) 863–884, https://doi.org/10.1001/jama.2020.0734.
[4] A.M. Noonan, S.H.M. Brown, Paraspinal muscle pathophysiology associated with low back pain and spine degenerative disorders, JOR Spine 4 (2021) e1171, https://doi.org/10.1002/jsp2.1171.
[5] M. Suo, J. Zhang, T. Sun, J. Wang, X. Liu, H. Huang, Z. Li, The association between morphological characteristics of paraspinal muscle and spinal disorders, Ann. Med. 55 (2023) 2258922, https://doi.org/10.1080/07853890.2023.2258922.
[6] H.W.D. Hey, W.M.R. Lam, C.X. Chan, W.H. Zhuo, E.M. Crombie, T.C. Tan, W.C. Chen, S. Cool, S.Y. Tsai, Paraspinal myopathy-induced intervertebral disc degeneration and thoracolumbar kyphosis in TSC1mKO mice model-a preliminary study, Spine J. 22 (2022) 483–494, https://doi.org/10.1016/j.spinee.2021.09.003.
[7] M.V. Risbud, I.M. Shapiro, Role of cytokines in intervertebral disc degeneration: pain and disc content, Nat. Rev. Rheumatol. 10 (2014) 44–56, https://doi.org/10.1038/nrrheum.2013.160.
[8] M.M. Panjabi, The stabilizing system of the spine. Part I. Function, dysfunction, adaptation, and enhancement, J. Spinal Disord. 5 (1992) 383–389, https://doi.org/10.1097/00002517-199212000-00001.
[9] M.M. Panjabi, The stabilizing system of the spine. Part II. Neutral zone and instability hypothesis, J. Spinal Disord. 5 (1992) 390–396, https://doi.org/10.1097/00002517-199212000-00002.
[10] A. Qaseem, T.J. Wilt, R.M. McLean, M.A. Forciea, T.D. Denberg, M.J. Barry, C. Boyd, R.D. Chow, N. Fitterman, R.P. Harris, L.L. Humphrey, S. Vijan, Noninvasive treatments for acute, subacute, and chronic low back pain: a clinical practice guideline from the American college of physicians, Ann. Intern. Med. 166 (2017) 514–530, https://doi.org/10.7326/M16-2367.
[11] N.E. Foster, J.R. Anema, D. Cherkin, R. Chou, S.P. Cohen, D.P. Gross, P.H. Ferreira, J.M. Fritz, B.W. Koes, W. Peul, J.A. Turner, C.G. Maher, Lancet Low Back Pain Series Working Group, Prevention and treatment of low back pain: evidence, challenges, and promising directions, Lancet 391 (2018) 2368–2383, https://doi.org/10.1016/S0140-6736(18)30489-6.
[12] T. Ohnishi, N. Iwasaki, H. Sudo, Causes of and molecular targets for the treatment of intervertebral disc degeneration: a review, Cells 11 (2022) 394, https://doi.org/10.3390/cells11030394.
[13] Y. Li, D. Pan, X. Wang, Z. Huo, X. Wu, J. Li, J. Cao, H. Xu, L. Du, B. Xu, Silencing ATF3 might delay TBHP-induced intervertebral disc degeneration by repressing NPC ferroptosis, apoptosis, and ECM degradation, Oxid. Med. Cell. Longev. 2022 (2022) 4235126, https://doi.org/10.1155/2022/4235126.
[14] Y. Li, X. Wu, J. Li, L. Du, X. Wang, J. Cao, H. Li, Z. Huo, G. Li, D. Pan, H. Xu, B. Xu, Circ_0004354 might compete with circ_0040039 to induce NPCs death and inflammatory response by targeting miR-345-3p-FAF1/TP73 axis in intervertebral disc degeneration, Oxid. Med. Cell. Longev. 2022 (2022) 2776440, https://doi.org/10.1155/2022/2776440.
[15] Y. Li, B. Wang, W. Sun, C. Kong, J. Ding, F. Hu, J. Li, X. Chen, S. Lu, Construction of circ_0071922-miR-15a-5p-mRNA network in intervertebral disc degeneration by RNA-sequencing, JOR Spine 7 (2023) e1275, https://doi.org/10.1002/jsp2.1275.
[16] Y. Li, C. Kong, W. Wang, F. Hu, X. Chen, B. Xu, S. Lu, Screening of miR-15a-5p as a potential biomarker for intervertebral disc degeneration through RNA-sequencing, Int. Immunopharm. 123 (2023) 110717, https://doi.org/10.1016/j.intimp.2023.110717.
[17] Y. Huang, L. Wang, B. Luo, K. Yang, X. Zeng, J. Chen, Z. Zhang, Y. Li, X. Cheng, B. He, Associations of lumber disc degeneration with paraspinal muscles myosteatosis in discogenic low back pain, Front. Endocrinol. 13 (2022) 891088, https://doi.org/10.3389/fendo.2022.891088.

[18] Y. Huang, L. Wang, X. Zeng, J. Chen, Z. Zhang, Y. Jiang, L. Nie, X. Cheng, B. He, Association of paraspinal muscle CSA and PDFF measurements with lumbar intervertebral disk degeneration in patients with chronic low back pain, Front. Endocrinol. 13 (2022) 792819, https://doi.org/10.3389/fendo.2022.792819.
[19] X. Wang, R. Jia, J. Li, Y. Zhu, H. Liu, W. Wang, Y. Sun, F. Zhang, L. Guo, W. Zhang, Research progress on the mechanism of lumbarmultifidus injury and degeneration, Oxid. Med. Cell. Longev. 2021 (2021) 6629037, https://doi.org/10.1155/2021/6629037.
[20] Z. Cheng, Y. Li, M. Li, J. Huang, J. Huang, Y. Liang, S. Lu, C. Liang, T. Xing, K. Su, G. Wen, W. Zeng, L. Huang, Correlation between posterior paraspinal muscle atrophy and lumbar intervertebral disc degeneration in patients with chronic low back pain, Int. Orthop. 47 (2023) 793–801, https://doi.org/10.1007/s00264-022-05621-9.
[21] M. Minetama, M. Kawakami, T. Nakatani, M. Teraguchi, M. Nakagawa, Y. Yamamoto, S. Matsuo, N. Sakon, Y. Nakagawa, Lumbar paraspinal muscle morphology is associated with spinal degeneration in patients with lumbar spinal stenosis, Spine J. 23 (2023) 1630–1640, https://doi.org/10.1016/j.spinee.2023.06.398.
[22] Y. Li, C. Kong, B. Wang, W. Sun, X. Chen, W. Zhu, J. Ding, S. Lu, Identification of differentially expressed genes in mouse paraspinal muscle in response to microgravity, Front. Endocrinol. 13 (2022) 1020743, https://doi.org/10.3389/fendo.2022.1020743.
[23] J. Li, M. Tang, G. Yang, L. Wang, Q. Gao, H. Zhang, Muscle injury associated elevated oxidative stress and abnormal myogenesis in patients with idiopathic scoliosis, Int. J. Biol. Sci. 15 (2019) 2584–2595, https://doi.org/10.7150/ijbs.33340.
[24] X. Li, C.Y. Wang, From bulk, single-cell to spatial RNA sequencing, Int. J. Oral Sci. 13 (2021) 36, https://doi.org/10.1038/s41368-021-00146-0.
[25] D. Jovic, X. Liang, H. Zeng, L. Lin, F. Xu, Y. Luo, Single-cell RNA sequencing technologies and applications: a brief overview, Clin. Transl. Med. 12 (2022) e694, https://doi.org/10.1002/ctm2.694.
[26] E. Papalexi, R. Satija, Single-cell RNA sequencing to explore immune cell heterogeneity, Nat. Rev. Immunol. 18 (2018) 35–45, https://doi.org/10.1038/nri.2017.76.
[27] G. Han, Y. Jiang, B. Zhang, C. Gong, W. Li, Imaging evaluation of fat infiltration in paraspinal muscles on mri: a systematic review with a focus on methodology, Orthop. Surg. 13 (2021) 1141–1148, https://doi.org/10.1111/os.12962.
[28] Q. Li, L. Shi, Y. Wang, T. Guan, X. Jiang, D. Guo, J. Lv, L. Cai, A nomogram for predicting the residual back pain after percutaneous vertebroplasty for osteoporotic vertebral compression fractures, Pain Res. Manag. 2021 (2021) 3624614, https://doi.org/10.1155/2021/3624614.
[29] P.J. Battaglia, Y. Maeda, A. Welk, B. Hough, N. Kettner, Reliability of the Goutallier classification in quantifying muscle fatty degeneration in the lumbar multifidus using magnetic resonance imaging, J. Manip. Physiol. Ther. 37 (2014) 190–197, https://doi.org/10.1016/j.jmpt.2013.12.010.
[30] Z. Yin, J. Lin, R. Yan, R. Liu, M. Liu, B. Zhou, W. Zhou, C. An, Y. Chen, Y. Hu, C. Fan, K. Zhao, B. Wu, X. Zou, J. Zhang, A.H. El-Hashash, X. Chen, H. Ouyang, Atlas of musculoskeletal stem cells with the soft and hard tissue differentiation architecture, Adv. Sci. 7 (2020) 2000938, https://doi.org/10.1002/advs.202000938.
[31] A.J. De Micheli, J.A. Spector, O. Elemento, B.D. Cosgrove, A reference single-cell transcriptomic atlas of human skeletal muscle tissue reveals bifurcated muscle stem cell populations, Skeletal Muscle 10 (2020) 19, https://doi.org/10.1186/s13395-020-00236-3.
[32] L. Giordani, G.J. He, E. Negroni, H. Sakai, J.Y.C. Law, M.M. Siu, R. Wan, A. Corneau, S. Tajbakhsh, T.H. Cheung, F. Le Grand, High-dimensional single-cell cartography reveals novel skeletal muscle-resident cell populations, Mol. Cell 74 (2019) 609–621.e6, https://doi.org/10.1016/j.molcel.2019.02.026.
[33] D. Szklarczyk, R. Kirsch, M. Koutrouli, K. Nastou, F. Mehryary, R. Hachilif, A.L. Gable, T. Fang, N.T. Doncheva, S. Pyysalo, P. Bork, L.J. Jensen, C. von Mering, The STRING database in 2023: protein-protein association networks and functional enrichment analyses for any sequenced genome of interest, Nucleic Acids Res. 51 (2023) D638–D646, https://doi.org/10.1093/nar/gkac1000.
[34] Y. Li, B. Wang, W. Sun, C. Kong, G. Li, X. Chen, S. Lu, Screening the immune-related circRNAs and genes in mice of spinal cord injury by RNA sequencing, Front. Immunol. 13 (2022) 1060290, https://doi.org/10.3389/fimmu.2022.1060290.
[35] N. Zhou, J. Bao, FerrDb: a manually curated resource for regulators and markers of ferroptosis and ferroptosis-disease associations, Database 2020 (2020) baaa021, https://doi.org/10.1093/database/baaa021.
[36] A. Liberzon, C. Birger, H. Thorvaldsdóttir, M. Ghandi, J.P. Mesirov, P. Tamayo, The Molecular Signatures Database (MSigDB) hallmark gene set collection, Cell Syst 1 (2015) 417–425, https://doi.org/10.1016/j.cels.2015.12.004.
[37] S. Bhattacharya, P. Dunn, C.G. Thomas, B. Smith, H. Schaefer, J. Chen, Z. Hu, K.A. Zalocusky, R.D. Shankar, S.S. Shen-Orr, E. Thomson, J. Wiser, A.J. Butte, ImmPort, toward repurposing of open access immunological assay data for translational and clinical research, Sci. Data 5 (2018) 180015, https://doi.org/10.1038/sdata.2018.15.
[38] S.E. McGeary, K.S. Lin, C.Y. Shi, T.M. Pham, N. Bisaria, G.M. Kelley, D.P. Bartel, The biochemical basis of microRNA targeting efficacy, Science 366 (2019) eaav1741, https://doi.org/10.1126/science.aav1741.
[39] A.C. Hauschild, C. Pastrello, G.K.A. Ekaputeri, D. Bethune-Waddell, M. Abovsky, Z. Ahmed, M. Kotlyar, R. Lu, I. Jurisica, MirDIP 5.2: tissue context annotation and novel microRNA curation, Nucleic Acids Res. 51 (2023) D217–D225, https://doi.org/10.1093/nar/gkac1070.
[40] X. Robin, N. Turck, A. Hainard, N. Tiberti, F. Lisacek, J.C. Sanchez, M. Müller, pROC: an open-source package for R and S+ to analyze and compare ROC curves, BMC Bioinf. 12 (2011) 77, https://doi.org/10.1186/1471-2105-12-77.
[41] Z. Xu, W. You, W. Chen, Y. Zhou, Q. Nong, T.G. Valencak, Y. Wang, T. Shan, Single-cell RNA sequencing and lipidomics reveal cell and lipid dynamics of fat infiltration in skeletal muscle, J Cachexia Sarcopenia Muscle 12 (2021) 109–129, https://doi.org/10.1002/jcsm.12643.
[42] A.J. De Micheli, E.J. Laurilliard, C.L. Heinke, H. Ravichandran, P. Fraczek, S. Soueid-Baumgarten, I. De Vlaminck, O. Elemento, B.D. Cosgrove, Single-cell analysis of the muscle stem cell hierarchy identifies heterotypic communication signals involved in skeletal muscle regeneration, Cell Rep. 30 (2020) 3583–3595.e5, https://doi.org/10.1016/j.celrep.2020.02.067.
[43] F.S. Nahm, Receiver operating characteristic curve: overview and practical use for clinicians, Korean J Anesthesiol 75 (2022) 25–36, https://doi.org/10.4097/kja.21209.
[44] S. Dell'Orso, A.H. Juan, K.D. Ko, F. Naz, J. Perovanovic, G. Gutierrez-Cruz, X. Feng, V. Sartorelli, Single cell analysis of adult mouse skeletal muscle stem cells in homeostatic and regenerative conditions, Development 146 (2019) dev174177, https://doi.org/10.1242/dev.174177.
[45] L. Zhang, X. Yu, L. Zheng, Y. Zhang, Y. Li, Q. Fang, R. Gao, B. Kang, Q. Zhang, J.Y. Huang, H. Konno, X. Guo, Y. Ye, S. Gao, S. Wang, X. Hu, X. Ren, Z. Shen, W. Ouyang, Z. Zhang, Lineage tracking reveals dynamic relationships of T cells in colorectal cancer, Nature 564 (2018) 268–272, https://doi.org/10.1038/s41586-018-0694-x.
[46] P.T.B. Ho, I.M. Clark, L.T.T. Le, MicroRNA-based diagnosis and therapy, Int. J. Mol. Sci. 23 (2022) 7167, https://doi.org/10.3390/ijms23137167.
[47] C. Diener, A. Keller, E. Meese, Emerging concepts of miRNA therapeutics: from cells to clinic, Trends Genet. 38 (2022) 613–626, https://doi.org/10.1016/j.tig.2022.02.006.
[48] J.S. Chamberlain, A boost for muscle with gene therapy, N. Engl. J. Med. 386 (2022) 1184–1186, https://doi.org/10.1056/NEJMcibr2118576.
[49] A.R. Gillies, R.L. Lieber, Structure and function of the skeletal muscle extracellular matrix, Muscle Nerve 44 (2011) 318–331, https://doi.org/10.1002/mus.22094.
[50] P.P. Purslow, The structure and role of intramuscular connective tissue in muscle function, Front. Physiol. 11 (2020) 495, https://doi.org/10.3389/fphys.2020.00495.
[51] M. Gumpenberger, B. Wessner, A. Graf, M.V. Narici, C. Fink, S. Braun, C. Hoser, A.J. Blazevich, R. Csapo, Remodeling the skeletal muscle extracellular matrix in older age-effects of acute exercise stimuli on gene expression, Int. J. Mol. Sci. 21 (2020) 7089, https://doi.org/10.3390/ijms21197089.
[52] I. Kramerova, C. Kumagai-Cresse, N. Ermolova, E. Mokhonova, M. Marinov, J. Capote, D. Becerra, M. Quattrocelli, R.H. Crosbie, E. Welch, E.M. McNally, M. J. Spencer, Spp1 (osteopontin) promotes TGFβ processing in fibroblasts of dystrophin-deficient muscles through matrix metalloproteinases, Hum. Mol. Genet. 28 (2019) 3431–3442, https://doi.org/10.1093/hmg/ddz181.
[53] G.Z. Zhang, Y.J. Deng, Q.Q. Xie, E.H. Ren, Z.J. Ma, X.G. He, Y.C. Gao, X.W. Kang, Sirtuins and intervertebral disc degeneration: roles in inflammation, oxidative stress, and mitochondrial function, Clin. Chim. Acta 508 (2020) 33–42, https://doi.org/10.1016/j.cca.2020.04.016.
[54] E. Sziksz, D. Pap, R. Lippai, N.J. Béres, A. Fekete, A.J. Szabó, Á. Vannay, Fibrosis related inflammatory mediators: role of the IL-10 cytokine family, Mediat. Inflamm. 2015 (2015) 764641, https://doi.org/10.1155/2015/764641.

[55] S. Panni, R.C. Lovering, P. Porras, S. Orchard, Non-coding RNA regulatory networks, Biochim Biophys Acta Gene Regul Mech. 1863 (2020) 194417, https://doi.org/10.1016/j.bbagrm.2019.194417.

[56] J. Täubel, W. Hauke, S. Rump, J. Viereck, S. Batkai, J. Poetzsch, L. Rode, H. Weigt, C. Genschel, U. Lorch, C. Theek, A.A. Levin, J. Bauersachs, S.D. Solomon, T. Thum, Novel antisense therapy targeting microRNA-132 in patients with heart failure: results of a first-in-human Phase 1b randomized, double-blind, placebo-controlled study, Eur. Heart J. 42 (2021) 178–188, https://doi.org/10.1093/eurheartj/ehaa898.

[57] S. Batkai, C. Genschel, J. Viereck, S. Rump, C. Bär, T. Borchert, D. Traxler, M. Riesenhuber, A. Spannbauer, D. Lukovic, K. Zlabinger, E. Hašimbegović, J. Winkler, R. Garamvölgyi, S. Neitzel, M. Gyöngyösi, T. Thum, CDR132L improves systolic and diastolic function in a large animal model of chronic heart failure, Eur. Heart J. 42 (2021) 192–201, https://doi.org/10.1093/eurheartj/ehaa791.